Robotica (1997) volume 15, pp 385–394. Printed in the United Kingdom © 1997 Cambridge University Press

Kinematics and dynamics of a six-degree-of-freedom parallel manipulator with revolute legs

Kourosh E. Zanganeh*, Rosario Sinatra† and Jorge Angeles‡

SUMMARY

This paper presents the kinematics and dynamics of a six-degree-of-freedom platform-type parallel manipulator with six revolute legs, i.e. each leg consists of two links that are connected by a revolute joint. Moreover, each leg is connected, in turn, to the base and moving platforms by means of universal and spherical joints, respectively. We first introduce a kinematic model for the manipulator under study. Then, this model is used to derive the kinematics relations of the manipulator at the displacement, velocity and acceleration levels. Based on the proposed model, we develop the dynamics equations of the manipulator using the method of the natural orthogonal complement. The implementation of the model is illustrated by computer simulation and numerical results are presented for a sample trajectory in the Cartesian space.

KEYWORDS: Parallel manipulator; Revolute legs; Kinematics and dynamics; Natural orthogonal complement.

1 INTRODUCTION

The conventional six-degree-of-freedom (six-dof) platform-type parallel manipulator, commonly called Stewart or Stewart-Gough platform,[1] consists of a moving platform (MP) that is connected by six telescopic legs to a base platform (BP), as depicted in Fig. 1. Moreover, six actuators of the legs are used to control the motion of the manipulator.

The parallel structure of the Stewart platform, as compared to the structure of serial manipulators, has higher stiffness and better dynamic-response characteristics, since the overall load on the system is more evenly distributed among the actuators. However, the workspace of the manipulator is considerably small, which, to some extent, limits the full exploitation of these predominant features. Nevertheless, one can increase the useful volume of the workspace by a proper redesign of the legs, e.g. by replacing prismatic with revolute joints and changing the actuators accordingly. In this way, the potential applications of the manipulator can be extended, while preserving its predominant features. The kinematic analysis of a six-dof parallel manipulator with three legs in an all-revolute design has been reported by Cleary and Brooks.[2] Each leg in their design is driven by two motors through a differential drive. Here, we consider a more general architecture comprising six two-link revolute legs, as depicted in Fig. 2. The legs are connected to the BP and MP by a set of universal and spherical joints, respectively. Moreover, the motion of the manipulator is controlled by six motors that are mounted on the base. Each motor actuates the corresponding leg through a coupling with one of the two axes of the universal joint. This unconventional design offers some advantages in terms of the motion characteristics and the workspace volume; revealing these properties calls for a more detailed analysis, which motivates the present work.

To better understand the features of any alternative manipulator design, a study of its dynamics, in parallel to a study of its kinematics, is an essential task. In recent years, extensive research has been reported on the kinematic analysis of the Stewart platform and its various versions,[3] but regarding its dynamics, the work reported is considerably scarcer. In this context, Sugimoto[4] proposed a method of inverse dynamics using motor algebra, while Do and Yang[5] introduced an inverse-dynamics algorithm based on the Newton-Euler equations. Other research work on this subject can be found in the pertinent literature.[6–14] However, most of these works focus on manipulators with prismatic legs.

In this paper, we propose a model for the kinematics of the manipulator shown in Fig. 2. This model is used, in turn, to derive the dynamics equations of the system based on the natural orthogonal complement (NOC), as proposed by Angeles and Lee.[15,16] Moreover, these equations are implemented in an algorithm that is used to study the kinematics and dynamics of the manipulator at hand. The application of this algorithm is illustrated through a numerical example that simulates the kinematics and dynamics behavior of a typical manipulator while following a sample trajectory.

2 KINEMATICS

With reference to Fig. 2, the origin of the coordinate frame $\mathcal{B}$ is fixed at point O of the BP, while a frame $\mathcal{M}$ is assigned to the MP with its origin at point P. Let us now consider the ith leg of the manipulator, as shown in Fig. 3. In this figure, a motor is coupled to the axis $\mathcal{L}_i$ of the universal joint, and used to actuate this leg. The leg itself consists of two links of length $l_i \equiv \|\overrightarrow{A_iR_i}\|$ and $s_i \equiv \|\overrightarrow{R_iB_i}\|$, which are free to rotate about $\mathcal{A}_i$ and $\mathcal{R}_i$ axes, respectively. Since these two axes are parallel, the motion of the foregoing links are confined to the Π_i

* Institute for Aerospace Studies, University of Toronto, Downsview, Ontario (Canada) M3H 5T6 *kez@sdr.utias.utoronto.ca.*
† Istituto di Macchine, Facoltà d'Ingegneria, Università di Catania, Viale A. Doria 6, 95125 Catania (Italy) *rsinatra@im.ing.unict.it.*
‡ Department of Mechanical Engineering & Centre for Intelligent Machines, McGill University, Montreal, Quebec (Canada) H3A 2K6 *E-mail: angeles@cim.mcgill.ca.*

https://doi.org/10.1017/S0263574797000477 Published online by Cambridge University Press

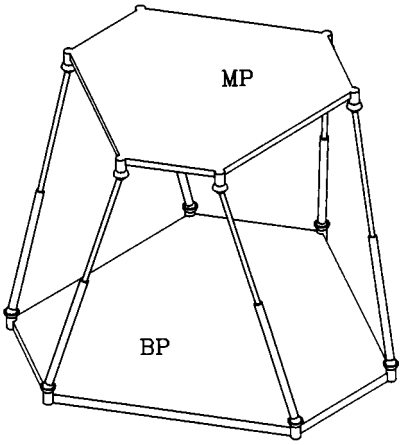

Fig. 1. The six-dof parallel manipulator with prismatic legs.

plane passing through the center of the ith universal joint and perpendicular to the aforementioned axes.

Next, we define two coordinate frames $\hat{\mathcal{B}}_i(\hat{x}_i, \hat{y}_i, \hat{z}_i)$ and $\mathcal{F}_i(x_i, y_i, z_i)$, with their origins fixed at point A_i, such that the x_i- and the y_i-axis of frame $\mathcal{F}_i$ are directed along $\mathcal{A}_i$ and $\mathcal{L}_i$ axes, respectively, while the z_i-axis lies in the Π_i plane. Moreover, frame $\mathcal{F}_i$ is confined to rotate about the $\hat{y}_i$-axis of the fixed frame $\hat{\mathcal{B}}_i$, its angle of rotation being φ_i. Thus, the rotation matrix $\boldsymbol{Q}_i$ that represents the orientation of $\mathcal{F}_i$ with respect to $\hat{\mathcal{B}}_i$ is given as

$$\boldsymbol{Q}_i \equiv \begin{bmatrix} \cos\varphi_i & 0 & -\sin\varphi_i \\ 0 & 1 & 0 \\ \sin\varphi_i & 0 & \cos\varphi_i \end{bmatrix}; \qquad i = 1, \ldots, 6 \qquad (1)$$

Furthermore, unit vectors along each of the three mutually perpendicular axes of frame $\hat{\mathcal{B}}_i$ are defined as

$$\hat{\boldsymbol{y}}_i \equiv \boldsymbol{u}_i = [u_i, v_i, 0]^T;$$
$$\hat{\boldsymbol{z}}_i \equiv \boldsymbol{z} = [0, 0, 1]^T; \qquad \hat{\boldsymbol{x}}_i \equiv \hat{\boldsymbol{y}}_i \times \hat{\boldsymbol{z}}_i \qquad (2a)$$

where $\boldsymbol{u}_i$ is a unit vector along the $\mathcal{L}_i$-axis. Likewise, the rotation matrix $\hat{\boldsymbol{Q}}_i$ that represents the orientation of $\hat{\mathcal{B}}_i$ with respect to $\mathcal{B}$, for $i = 1, \ldots, 6$, can be expressed in the $\mathcal{B}$-frame as

$$\hat{\boldsymbol{Q}}_i \equiv [\hat{\boldsymbol{x}}_i, \hat{\boldsymbol{y}}_i, \hat{\boldsymbol{z}}_i] = \begin{bmatrix} v_i & u_i & 0 \\ -u_i & v_i & 0 \\ 0 & 0 & 1 \end{bmatrix}; \qquad i = 1, \ldots, 6 \qquad (2b)$$

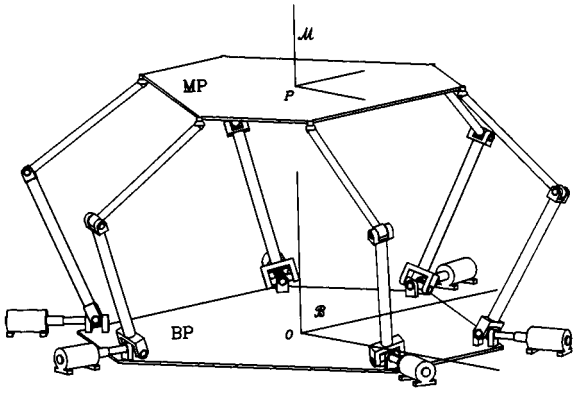

Fig. 2. The six-dof parallel manipulator with revolute legs.

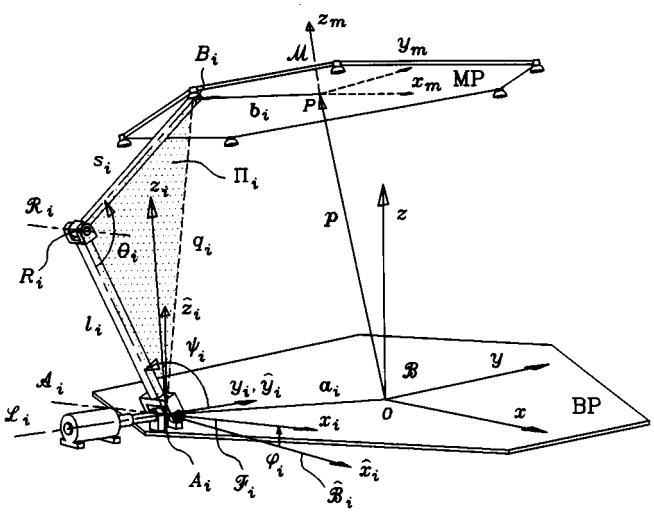

Fig. 3. Kinematic notation of the ith revolute leg.

Referring to Fig. 3, we can readily derive the relation below:

$$\overrightarrow{A_iB_i} \equiv \overrightarrow{A_iR_i} + \overrightarrow{R_iB_i} = -\boldsymbol{a}_i + \boldsymbol{p} + \boldsymbol{Q}\boldsymbol{b}_i; \quad i = 1, \ldots, 6 \qquad (3)$$

where $\boldsymbol{a}_i$ and $\boldsymbol{p}$ are the position vectors of A_i and P in frame $\mathcal{B}$, while $\boldsymbol{b}_i$ is the position vector of B_i in frame $\mathcal{M}$. Moreover, $\boldsymbol{Q}$ represents the rotation matrix relating the orientation of $\mathcal{M}$ with respect to that of $\mathcal{B}$. Using the trigonometric relations in triangle $A_iR_iB_i$, for $i = 1, \ldots, 6$, we can readily derive the expressions below:

$$\theta_i = \cos^{-1}[(l_i^2 + s_i^2 - q_i^2)/(2l_is_i)] \qquad (4a)$$

$$\dot{\theta}_i = (\dot{q}_iq_i)/(l_is_i \sin\theta_i) \qquad (4b)$$

$$\ddot{\theta}_i = (q_i^2 + q_i\ddot{q}_i - l_is_i\dot{\theta}_i^2 \cos\theta_i)/(l_is_i \sin\theta_i) \qquad (4c)$$

where $q_i \equiv \|\overrightarrow{A_iB_i}\|$, with $\|\cdot\|$ denoting the Euclidean norm of $(\cdot)$. Moreover, using equation (3) we can write

$$q_i^2 = (\boldsymbol{a}_i + \boldsymbol{p} + \boldsymbol{Q}\boldsymbol{b}_i)^T(\boldsymbol{a}_i + \boldsymbol{p} + \boldsymbol{Q}\boldsymbol{b}_i); \quad i = 1, \ldots, 6 \qquad (5)$$

upon differentiating both sides of equation (5) with respect to time, we obtain

$$\dot{q}_i \equiv dq_i/dt = \frac{1}{q_i}(\dot{\boldsymbol{p}} + \boldsymbol{\Omega}\boldsymbol{Q}\boldsymbol{b}_i)^T\overrightarrow{A_iB_i}; \quad i = 1, \ldots, 6 \qquad (6)$$

In the above equation, $\boldsymbol{\Omega}$ denotes the angular-velocity matrix of the MP, its associated angular-velocity vector $\boldsymbol{\omega}$ being given as

$$\boldsymbol{\omega} \equiv \begin{bmatrix} \omega_x \\ \omega_y \\ \omega_z \end{bmatrix} = \text{vect}(\boldsymbol{\Omega}) \equiv \frac{1}{2}\begin{bmatrix} \omega_{32} - \omega_{23} \\ \omega_{13} - \omega_{31} \\ \omega_{21} - \omega_{12} \end{bmatrix} \qquad (7)$$

where ω_{ij}, for $i = 1, 2, 3$ and $j = 1, 2, 3$, denotes the entry in the ith row and the jth column of matrix $\boldsymbol{\Omega}$. Further differentiation of equation (6) with respect to time leads to the relation

$$\ddot{q}_i \equiv d^2q_i/dt^2 = \frac{1}{q_i}\{\|\dot{\boldsymbol{p}} + \boldsymbol{\Omega}\boldsymbol{Q}\boldsymbol{b}_i\|^2 + [\ddot{\boldsymbol{p}} + (\dot{\boldsymbol{\Omega}} + \boldsymbol{\Omega}^2)\boldsymbol{Q}\boldsymbol{b}_i]^T\overrightarrow{A_iB_i} - \dot{q}_i^2\} \qquad (8)$$

where $\dot{\boldsymbol{\Omega}}$ is the cross-product matrix of $\dot{\boldsymbol{\omega}} \equiv [\dot{\omega}_x, \dot{\omega}_y, \dot{\omega}_z]^T$, with $\dot{\boldsymbol{\omega}}$ being the angular-acceleration vector of the MP.

https://doi.org/10.1017/S0263574797000477 Published online by Cambridge University Press

On the other hand, vectors $\overrightarrow{A_iR_i}$ and $\overrightarrow{R_iB_i}$, when expressed in frame $\mathcal{F}_i$, take on the forms

$$[\overrightarrow{A_iR_i}]_i = \begin{bmatrix} 0 \\ l_i \cos\psi_i \\ l_i \sin\psi_i \end{bmatrix}; \quad [\overrightarrow{R_iB_i}]_i = \begin{bmatrix} 0 \\ -s_i \cos(\psi_i + \theta_i) \\ -s_i \sin(\psi_i + \theta_i) \end{bmatrix}; \quad i = 1, \ldots, 6 \tag{9}$$

where $[\cdot]_i$ is the representation of any vector or matrix $(\cdot)$ in frame $\mathcal{F}_i$. In addition, ψ_i denotes the angle between the positive direction of $\hat{\mathbf{y}}_i$ and $\overrightarrow{A_iR_i}$ (see Fig. 3). Moreover, using equation (3) we can write

$$\overrightarrow{A_iB_i} \equiv \hat{\boldsymbol{Q}}_i \boldsymbol{Q}_i [\overrightarrow{A_iB_i}]_i = -\boldsymbol{a}_i + \boldsymbol{p} + \boldsymbol{Q}\boldsymbol{b}_i; \quad i = 1, \ldots, 6 \tag{10}$$

Now, upon differentiating both sides of equation (10) with respect to time, and rearranging of terms, we obtain

$$\frac{d}{dt}[\overrightarrow{A_iB_i}]_i = \boldsymbol{h}_i - \boldsymbol{\Omega}_i [\overrightarrow{A_iB_i}]_i; \qquad i = 1, \ldots, 6 \tag{11a}$$

where vector $\boldsymbol{h}_i$, for $i = 1, \ldots, 6$, is defined as

$$\boldsymbol{h}_i \equiv [h_{ix}, h_{iy}, h_{iz}]^T = \boldsymbol{Q}_i^T \hat{\boldsymbol{Q}}_i^T (\dot{\boldsymbol{p}} + \boldsymbol{\Omega}\boldsymbol{Q}\boldsymbol{b}_i) \tag{11b}$$

Moreover, $\boldsymbol{\Omega}_i$ represents the angular-velocity matrix of frame $\mathcal{F}_i$, its associated angular-velocity vector, $\boldsymbol{\omega}_i$, being given as

$$\boldsymbol{\omega}_i \equiv [0, -\dot{\varphi}_i, 0]^T = \text{vect}(\boldsymbol{\Omega}_i) \tag{12}$$

Now, if we let $\boldsymbol{k}_i \equiv [k_{ix}, k_{iy}, k_{iz}]^T = \hat{\boldsymbol{Q}}_i^T(-\boldsymbol{a}_i + \boldsymbol{p} + \boldsymbol{Q}\boldsymbol{b}_i)$, then equations (9 & 10) lead to the relation

$$[\overrightarrow{A_iB_i}]_i \equiv \begin{bmatrix} 0 \\ l_i \cos\psi_i - s_i \cos(\psi_i + \theta_i) \\ l_i \sin\psi_i - s_i \sin(\psi_i + \theta_i) \end{bmatrix} = \begin{bmatrix} k_{ix}\cos\varphi_i + k_{iz}\sin\varphi_i \\ k_{iy} \\ -k_{ix}\sin\varphi_i + k_{iz}\cos\varphi_i \end{bmatrix} \tag{13}$$

Furthermore, assuming that $0 \leq \varphi_i, \psi_i \leq \pi$, we can readily compute φ_i and ψ_i from the first two components of vector $[\overrightarrow{A_iB_i}]_i$ in equation (13), for $i = 1, \ldots, 6$, as

$$\varphi_i = -\tan^{-1}(k_{ix}/k_{iz}) \tag{14a}$$

$$\psi_i = \text{atan}(s_i \sin\theta_i, l_i - s_i \cos\theta_i) + \text{atan}(\sqrt{q_i^2 - k_{iy}^2}, -k_{iy}) \tag{14b}$$

In the above equations, "atan" obviously denotes the two-argument arc-tangent function which sometimes represented by "atan2". In addition, we differentiate the left-hand side of equation (13) with respect to time and then equate the expression thus resulting with the right-hand side of equation (11a). In this way, two relations can be derived from the first two components of $d[\overrightarrow{A_iB_i}]_i/dt$, namely,

$$\dot{\varphi}_i = \frac{h_{ix}}{s_i \sin(\psi_i + \theta_i)}; \qquad i = 1, \ldots, 6 \tag{15a}$$

$$\dot{\psi}_i = \frac{h_{iy} - s_i\dot{\theta}_i \sin(\psi_i + \theta_i)}{-l_i \sin\psi_i + s_i \sin(\psi_i + \theta_i)}; \qquad i = 1, \ldots, 6 \tag{15b}$$

Now, the angular-velocity vectors of the two links of the ith leg, i.e., $\boldsymbol{\nu}_i$ and $\boldsymbol{\xi}_i$, for $i = 1, \ldots, 6$, are computed as

$$\boldsymbol{\nu}_i = \hat{\boldsymbol{Q}}_i(\boldsymbol{Q}_i[\boldsymbol{\nu}_i]_i - \boldsymbol{\omega}_i); \qquad \boldsymbol{\xi}_i = \hat{\boldsymbol{Q}}_i(\boldsymbol{Q}_i[\boldsymbol{\xi}_i]_i - \boldsymbol{\omega}_i) \tag{16}$$

where, $[\boldsymbol{\nu}_i]_i \equiv [\dot{\psi}_i, 0, 0]^T$ and $[\boldsymbol{\xi}_i]_i \equiv [\dot{\psi}_i + \dot{\theta}_i, 0, 0]^T$. On the other hand, expressions for the angular-acceleration vectors of the same links can be obtained from equation (16) by differentiating both sides of the foregoing equations with respect to time, thereby obtaining

$$\dot{\boldsymbol{\nu}}_i = \hat{\boldsymbol{Q}}_i(\boldsymbol{\Omega}_i\boldsymbol{Q}_i[\boldsymbol{\nu}_i]_i + \boldsymbol{Q}_i[\dot{\boldsymbol{\nu}}_i]_i - \dot{\boldsymbol{\omega}}_i); \qquad i = 1, \ldots, 6 \tag{17a}$$

$$\dot{\boldsymbol{\xi}}_i = \hat{\boldsymbol{Q}}_i(\boldsymbol{\Omega}_i\boldsymbol{Q}_i[\boldsymbol{\xi}_i]_i + \boldsymbol{Q}_i[\dot{\boldsymbol{\xi}}_i]_i - \dot{\boldsymbol{\omega}}_i); \qquad i = 1, \ldots, 6 \tag{17b}$$

in which $\dot{\boldsymbol{\omega}}_i \equiv [0, -\ddot{\varphi}_i, 0]^T$. Moreover, to derive expressions for $\ddot{\varphi}_i$ and $\ddot{\psi}_i$, we first differentiate both sides of equation (11b) with respect to time, i.e.

$$d\boldsymbol{h}_i/dt \equiv [\dot{h}_{ix}, \dot{h}_{iy}, \dot{h}_{iz}]^T = \boldsymbol{Q}_i^T\hat{\boldsymbol{Q}}_i^T[\ddot{\boldsymbol{p}} + (\dot{\boldsymbol{\Omega}} + \boldsymbol{\Omega}^2)\boldsymbol{Q}\boldsymbol{b}_i] + (\hat{\boldsymbol{Q}}_i\boldsymbol{\Omega}_i\boldsymbol{Q}_i)^T(\dot{\boldsymbol{p}} + \boldsymbol{\Omega}\boldsymbol{Q}\boldsymbol{b}_i) \tag{18}$$

Then, upon differentiating both sides of equations (15a & b) with respect to time, for $i = 1, \ldots, 6$, we obtain

$$\ddot{\varphi}_i = \frac{\dot{h}_{ix} - \eta_i\varphi_i}{s_i \sin(\psi_i + \theta_i)} \tag{19a}$$

$$\ddot{\psi}_i = \frac{\dot{h}_{iy} - \eta_i\dot{\theta}_i - s_i\ddot{\theta}_i \sin(\psi_i + \theta_i) - (\eta_i - l_i\dot{\psi}_i \cos\psi_i)}{-l_i \sin\psi_i + s_i \sin(\psi_i + \theta_i)} \tag{19b}$$

where $\eta_i \equiv s_i(\dot{\psi}_i + \dot{\theta}_i)\cos(\psi_i + \theta_i)$.

2.1 The velocity Jacobians

It is known that the kinematic analysis of parallel manipulators leads to two Jacobian matrices.[17] Based on the role that these matrices play in the kinetostatic transformation between joint and Cartesian variables, they are commonly referred to as the *forward* and the *inverse* Jacobians. To find these Jacobians for the manipulator under study, we first use equation (11b) to derive the relation below:

$$h_{ix} \equiv [\boldsymbol{x}]_i^T\boldsymbol{h}_i = \boldsymbol{x}_i^T(\dot{\boldsymbol{p}} + \boldsymbol{\omega} \times \boldsymbol{Q}\boldsymbol{b}_i); \quad i = 1, \ldots, 6 \tag{20a}$$

in which, $[\boldsymbol{x}]_i \equiv [1, 0, 0]^T$ and $\boldsymbol{x}_i \equiv \hat{\boldsymbol{Q}}_i\boldsymbol{Q}_i[\boldsymbol{x}]_i$. After some algebraic operations, equation (20a) can be written in the form

$$h_{ix} \equiv \boldsymbol{x}_i^T\dot{\boldsymbol{p}} + (\boldsymbol{Q}\boldsymbol{b}_i \times \boldsymbol{x}_i)^T\boldsymbol{\omega}; \quad i = 1, \ldots, 6 \tag{20b}$$

Equation (20b), when substituted into equation (15a), leads to the relation

$$s_i\dot{\varphi}_i \sin(\psi_i + \theta_i) = [(\boldsymbol{Q}\boldsymbol{b}_i \times \boldsymbol{x}_i)^T \quad \boldsymbol{x}_i^T]\boldsymbol{t}_P; \quad i = 1, \ldots, 6 \tag{21}$$

https://doi.org/10.1017/S0263574797000477 Published online by Cambridge University Press

where $\boldsymbol{t}_P \equiv [\boldsymbol{\omega}^T, \dot{\boldsymbol{p}}^T]^T$ is the 6-dimensional twist array at point P of the MP. The six equations within equation (21) can be written in vector form as

$$\boldsymbol{A}\dot{\boldsymbol{\varphi}} = \boldsymbol{B}\boldsymbol{t}_P \tag{22}$$

in which, $\dot{\boldsymbol{\varphi}} = [\dot{\varphi}_1, \ldots, \dot{\varphi}_6]^T$ and the 6×6 matrices $\boldsymbol{A}$ and $\boldsymbol{B}$ are, in fact, the inverse and forward Jacobians of the manipulator, that are defined as

$$\boldsymbol{A} = \text{diag}\,(a_{11}, \ldots, a_{66}); \qquad \boldsymbol{B} = \begin{bmatrix} (\boldsymbol{Q}\boldsymbol{b}_1 \times \boldsymbol{x}_1)^T & \boldsymbol{x}_1^T \\ \vdots & \vdots \\ (\boldsymbol{Q}\boldsymbol{b}_6 \times \boldsymbol{x}_6)^T & \boldsymbol{x}_6^T \end{bmatrix} \tag{23}$$

where $a_{ii} \equiv s_i \sin(\psi_i + \theta_i)$, for $i = 1, \ldots, 6$. Now, we rewrite equation (22) in the form

$$\boldsymbol{T}\dot{\boldsymbol{\varphi}} = \boldsymbol{t}_P \tag{24}$$

where $\boldsymbol{T} \equiv \boldsymbol{B}^{-1}\boldsymbol{A}$. Hence, upon differentiating equation (24) with respect to time, we obtain

$$\boldsymbol{T}\ddot{\boldsymbol{\varphi}} + \dot{\boldsymbol{T}}\dot{\boldsymbol{\varphi}} = \dot{\boldsymbol{t}}_P \tag{25}$$

In the above equation, $\dot{\boldsymbol{t}}_P \equiv [\dot{\boldsymbol{\omega}}^T, \ddot{\boldsymbol{p}}^T]^T$, while $\dot{\boldsymbol{T}} \equiv \boldsymbol{B}^{-1}(\dot{\boldsymbol{A}} - \dot{\boldsymbol{B}}\boldsymbol{B}^{-1}\boldsymbol{A})$, with $\dot{\boldsymbol{A}}$ and $\dot{\boldsymbol{B}}$ given as

$$\dot{\boldsymbol{A}} = \text{diag}\,(\dot{a}_{11}, \ldots, \dot{a}_{66}); \qquad \dot{\boldsymbol{B}} = \begin{bmatrix} (\boldsymbol{\Omega}\boldsymbol{b}_1 \times \boldsymbol{x}_1 + \boldsymbol{Q}\boldsymbol{b}_1 \times \dot{\boldsymbol{x}}_1)^T & \dot{\boldsymbol{x}}_1^T \\ \vdots & \vdots \\ (\boldsymbol{\Omega}\boldsymbol{Q}\boldsymbol{b}_6 \times \boldsymbol{x}_6 + \boldsymbol{Q}\boldsymbol{b}_6 \times \dot{\boldsymbol{x}}_6)^T & \dot{\boldsymbol{x}}_6^T \end{bmatrix} \tag{26}$$

with $\dot{a}_{ii} \equiv s_i(\dot{\psi}_i + \dot{\theta}_i)\cos(\psi_i + \theta_i)$, and $\dot{\boldsymbol{x}}_i \equiv \hat{\boldsymbol{Q}}_i\boldsymbol{\Omega}_i\hat{\boldsymbol{Q}}_i^T\boldsymbol{x}_i$, for $i = 1, \ldots, 6$.

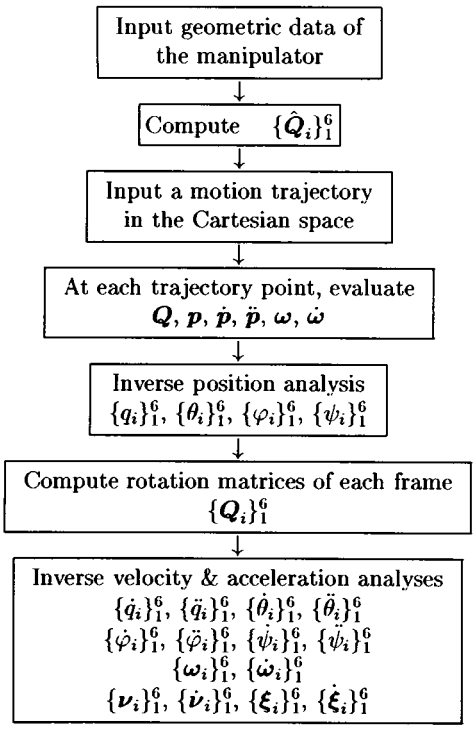

Fig. 4. Inverse-kinematics algorithm for the all-revolute manipulator.

2.2 Inverse kinematics

In the inverse kinematic problem, the motion of the end-effector is given and the corresponding motion of each joint, actuated or unactuated, is to be determined. The preceding kinematic modeling can be incorporated into a single algorithm to evaluate the inverse kinematics of the manipulator under different end-effector Cartesian trajectories. The basic steps of this algorithm are described in the diagram shown in Figure 4.

2.3 Direct kinematics

In the direct kinematics problem, the motion of each actuated joint is given and the corresponding end-effector motion as well as that of all unactuated joints are to be determined. At the outset, we find the solution to the direct problem at the displacement level. This is done by first substituting equation (5) into equation (4a). Thus, for $i = 1, \ldots, 6$, we obtain

$$l_i^2 + s_i^2 - 2l_i s_i \cos\theta_i = (\boldsymbol{a}_i + \boldsymbol{p} + \boldsymbol{Q}\boldsymbol{b}_i)^T(\boldsymbol{a}_i + \boldsymbol{p} + \boldsymbol{Q}\boldsymbol{b}_i) \tag{27}$$

The above equations, together with the twelve equations resulting from the first two rows of vector equations (13), yield 18 nonlinear equations in as many unknowns, namely, the three components of $\boldsymbol{p}$, the three independent entries of the rotation matrix $\boldsymbol{Q}$, $\{\theta_i\}_1^6$, and $\{\psi_i\}_1^6$. Once the pose of the end-effector, i.e. vector $\boldsymbol{p}$ and matrix $\boldsymbol{Q}$, and hence, the configuration of the manipulator is known at each instant, we can use equations (24) and (25) to compute the corresponding values for the components of $\boldsymbol{t}_p$ and $\dot{\boldsymbol{t}}_p$, respectively.

3 DYNAMICS MODELING USING THE NOC

In this section, we derive the equations of motion using the method of the natural orthogonal complement. With this method, a set of Euler–Lagrange equations, free of constraint forces, is derived from the Newton–Euler (NE) equations of all individual bodies, using the natural orthogonal complement of the coefficient matrix of the velocity constraint equations. This method was applied by Ma[9] for the modeling and simulation of the Stewart platform. Here, we adopt the same concept to develop a model for the manipulator under study.

At the outset, we recall the dynamics equations of a system that is composed of p rigid bodies coupled by holonomic constraints. The NE equations for every individual body can be written as

$$\boldsymbol{M}_i\dot{\boldsymbol{t}}_i = -\boldsymbol{W}_i\boldsymbol{M}_i\boldsymbol{t}_i + \boldsymbol{w}_i; \quad i = 1, \ldots, p \tag{28}$$

where $\boldsymbol{t}_i = [\boldsymbol{w}_i^T, \dot{\boldsymbol{c}}_i^T]^T$ is the 6-dimensional twist array of the ith body, defined in terms of its angular velocity, $\boldsymbol{\omega}_i$, and the velocity of the corresponding mass center, $\dot{\boldsymbol{c}}_i$. Moreover, if for the same body, $\boldsymbol{n}_i$ and $\boldsymbol{f}_i$ denote the resultant moment and the resultant force acting at the mass center, respectively, then $\boldsymbol{w}_i \equiv [\boldsymbol{n}_i^T, \boldsymbol{f}_i^T]^T$ represents the wrench acting on the body. This wrench can, in general, be decomposed into a working wrench and a nonworking constraint wrench, $\boldsymbol{w}_i^W$ and $\boldsymbol{w}_i^N$, respectively. Here, $\boldsymbol{w}_i^W$ comprises all moments and forces exerted by

https://doi.org/10.1017/S0263574797000477 Published online by Cambridge University Press

the environment, including motors and dissipative effects, while $\boldsymbol{w}_i^N$ comprises constraint moments and forces exerted by the neighboring bodies, and that do not produce any work, their sole role being to keep the bodies together. Now, the 6×6 *angular-velocity* dyad, $\boldsymbol{W}_i$, and the *inertia* dyad, $\mathbf{M}_i$, are defined as

$$\boldsymbol{W}_i \equiv \begin{bmatrix} \boldsymbol{\Omega}_i & \boldsymbol{O} \\ \boldsymbol{O} & \boldsymbol{O} \end{bmatrix}; \quad \boldsymbol{M}_i \equiv \begin{bmatrix} \boldsymbol{I}_i & \boldsymbol{O} \\ \boldsymbol{O} & m_i\mathbf{1} \end{bmatrix}; \qquad \boldsymbol{\Omega}_i \equiv \frac{\partial(\boldsymbol{\omega}_i \times \boldsymbol{v})}{\partial \boldsymbol{v}} = \boldsymbol{\omega}_i \times \mathbf{1} \tag{29}$$

where $\boldsymbol{I}_i$ denotes the 3×3 matrix of the ith body about its mass center, m_i represents the mass of the body and $\boldsymbol{v}$ is an arbitrary 3-dimensional vector. In addition, $\boldsymbol{O}$ and $\mathbf{1}$ are the zero and identity 3×3 matrices, respectively. It should be noted that the NE equations of the ith body are written with respect to a coordinate system fixed to the body. Next, the $6p\times 6p$ matrices of *generalized mass*, $\boldsymbol{M}$, and *generalized angular velocity*, $\boldsymbol{W}$, as well as the $6p$-dimensional vector of *generalized twist*, $\boldsymbol{t}$, *generalized working wrench*, $\boldsymbol{w}^W$, and *generalized nonworking wrench*, $\boldsymbol{w}^N$, are defined below:

$$\boldsymbol{t} \equiv \begin{bmatrix} \boldsymbol{t}_1 \\ \vdots \\ \boldsymbol{t}_p \end{bmatrix}; \quad \boldsymbol{w}^W \equiv \begin{bmatrix} \boldsymbol{w}_1^W \\ \vdots \\ \boldsymbol{w}_p^W \end{bmatrix}; \quad \boldsymbol{w}^N \equiv \begin{bmatrix} \boldsymbol{w}_1^N \\ \vdots \\ \boldsymbol{w}_p^N \end{bmatrix} \tag{30a}$$

$$\boldsymbol{M} \equiv \mathrm{diag}\,(\boldsymbol{M}_1, \ldots, \boldsymbol{M}_p); \quad \boldsymbol{W} \equiv \mathrm{diag}\,(\boldsymbol{W}_1, \ldots, \boldsymbol{W}_p) \tag{30b}$$

Hence, the $6p$ equations within equation (28) can be expressed in compact form as

$$\boldsymbol{M}\dot{\boldsymbol{t}} = -\boldsymbol{W}\boldsymbol{M}\boldsymbol{t} + \boldsymbol{w}^W + \boldsymbol{w}^N \tag{31}$$

The velocity constraint equations can be represented, in turn, by a system of linearly dependent equations on the vector of generalized twist, i.e., as $\boldsymbol{D}\boldsymbol{t} = \mathbf{0}_{6p}$, where $\mathbf{0}_{6p}$ is the $6p$-dimensional zero vector, $\boldsymbol{D}$ is a $6p\times 6p$ matrix of rank γ, with γ being the number of independent holonomic constraints. Thus, the degree of freedom of the system is readily computed as $n = 6p - \gamma$. Accordingly, a set of n independent variables exists that can play the role of independent *generalized speeds*.[18] If this set is stored in the n-dimensional array $\dot{\boldsymbol{\varphi}}$, then we can write:

$$\boldsymbol{t} = \boldsymbol{T}\dot{\boldsymbol{\varphi}} \tag{32a}$$

$$\dot{\boldsymbol{t}} = \boldsymbol{T}\ddot{\boldsymbol{\varphi}} + \dot{\boldsymbol{T}}\dot{\boldsymbol{\varphi}} \tag{32b}$$

where $\boldsymbol{T}$ is a $6p\times n$ twist-shaping matrix. Upon substituting for $\boldsymbol{t}$ into the velocity constraint equations, and recalling that all components of $\dot{\boldsymbol{\varphi}}$ are independent, we obtain

$$\boldsymbol{D}\boldsymbol{T} = \boldsymbol{O}_{6p\times n} \tag{33}$$

in which $\boldsymbol{T}$ is the natural orthogonal complement of $\boldsymbol{D}$. As discussed elsewhere,[15] $\boldsymbol{w}^N$ lies in the nullspace of the transpose of $\boldsymbol{T}$. Thus, if both sides of equation (31) are multiplied by $\boldsymbol{T}^T$ and equation (32b) is substituted into the equation thus resulting, we obtain

$$\boldsymbol{I}\ddot{\boldsymbol{\varphi}} + \boldsymbol{C}\dot{\boldsymbol{\varphi}} = \boldsymbol{T}^T\boldsymbol{w}^W \tag{34}$$

where the $n\times n$ matrices $\boldsymbol{I}$ and $\boldsymbol{C}$ are defined as:

$$\boldsymbol{I} \equiv \boldsymbol{T}^T\boldsymbol{M}\boldsymbol{T}; \quad \boldsymbol{C} \equiv \boldsymbol{T}^T(\boldsymbol{M}\dot{\boldsymbol{T}} + \boldsymbol{W}\boldsymbol{M}\boldsymbol{T})$$

On the other hand, $\boldsymbol{w}^N$ can be decomposed as follows:

$$\boldsymbol{w}^W = \boldsymbol{w}^a + \boldsymbol{w}^g + \boldsymbol{w}^d \tag{35}$$

where $\boldsymbol{w}^a$, $\boldsymbol{w}^g$ and $\boldsymbol{w}^d$ represent the generalized wrenches due to actuators, gravity and dissipative effects, respectively. Hence, equation (34) can be cast in the form

$$\boldsymbol{I}\ddot{\boldsymbol{\varphi}} + \boldsymbol{C}\dot{\boldsymbol{\varphi}} - \boldsymbol{\tau}^g - \boldsymbol{\tau}^d = \boldsymbol{\tau}^a \tag{36}$$

In the above equation, the n-dimensional generalized forces $\boldsymbol{\tau}^a$, $\boldsymbol{\tau}^g$ and $\boldsymbol{\tau}^d$ are defined as:

$$\boldsymbol{\tau}^a \equiv \boldsymbol{T}^T\boldsymbol{w}^a; \qquad \boldsymbol{\tau}^g \equiv \boldsymbol{T}^T\boldsymbol{w}^g; \quad \boldsymbol{\tau}^d \equiv \boldsymbol{T}^T\boldsymbol{w}^d$$

Equation (36) represents the Euler-Lagrange equations of the system, which are free of constraint forces. In the present form, equation (36) is suitable for the study of the direct dynamics of the manipulator. However, upon assembling all generalized inertia wrenches into vector $\boldsymbol{w}^n$, defined as $\boldsymbol{w}^n \equiv -\boldsymbol{M}\dot{\boldsymbol{t}} - \boldsymbol{W}\boldsymbol{M}\boldsymbol{t}$, equation (36) can be rewritten as

$$\boldsymbol{\tau}^a \equiv -\boldsymbol{T}^T(\boldsymbol{w}^n + \boldsymbol{w}^g + \boldsymbol{w}^d) \tag{37}$$

The dynamics model given by equation (37) is applicable in the solution of the inverse dynamics problem of the manipulator. The inertia wrench, $\boldsymbol{w}_i^n$ on the ith body can, in turn, be computed using the corresponding NE equation, i.e.,

$$\boldsymbol{w}_i^n \equiv \begin{bmatrix} -\boldsymbol{\omega}_i \times \boldsymbol{I}_i\boldsymbol{\omega}_i - \boldsymbol{I}_i\dot{\boldsymbol{\omega}}_i \\ -m_i\ddot{\boldsymbol{c}}_i \end{bmatrix} = -\boldsymbol{M}_i\dot{\boldsymbol{t}}_i - \boldsymbol{W}_i\boldsymbol{M}_i\boldsymbol{t}_i \tag{38}$$

where $\dot{\boldsymbol{\omega}}_i$ denotes the angular-acceleration vector of the ith body.

3.1 Dynamics analysis of the manipulator

In order to apply the dynamics model derived in the previous section, we need expressions for the twist of each body of the manipulator, along with the time-rate of change of this twist. Here, equations (16) and (17a & b) can be used to compute the angular velocity and angular acceleration of the ith-leg links. Moreover, for the MP, these vectors have been obtained as $\boldsymbol{\omega}$ and $\dot{\boldsymbol{\omega}}$, respectively, Referring to Figure 5, the position vectors of the mass centers of the foregoing bodies are given as

$$\boldsymbol{c}_i = \boldsymbol{a}_i + \rho_i\hat{\boldsymbol{Q}}_i\boldsymbol{Q}_i[\boldsymbol{e}_i]_i; \qquad i = 1, \ldots, 6 \tag{39a}$$

$$\boldsymbol{d}_i = \boldsymbol{a}_i + \hat{\boldsymbol{Q}}_i\boldsymbol{Q}_i\{l_i[\boldsymbol{e}_i]_i + \sigma_i[\boldsymbol{s}_i]_i\}; \quad i = 1, \ldots, 6 \tag{39b}$$

$$\boldsymbol{c} = \boldsymbol{p} + \boldsymbol{Q}\boldsymbol{\rho} \tag{39c}$$

where $[\boldsymbol{e}_i]_i \equiv [\overrightarrow{A_iR_i}]_i/l_i$, $[\boldsymbol{s}_i]_i \equiv [\overrightarrow{R_iB_i}]_i/s_i$, while $\boldsymbol{\rho}$ represents the position vector of the mass center of the MP in frame $\mathcal{M}$.

https://doi.org/10.1017/S0263574797000477 Published online by Cambridge University Press

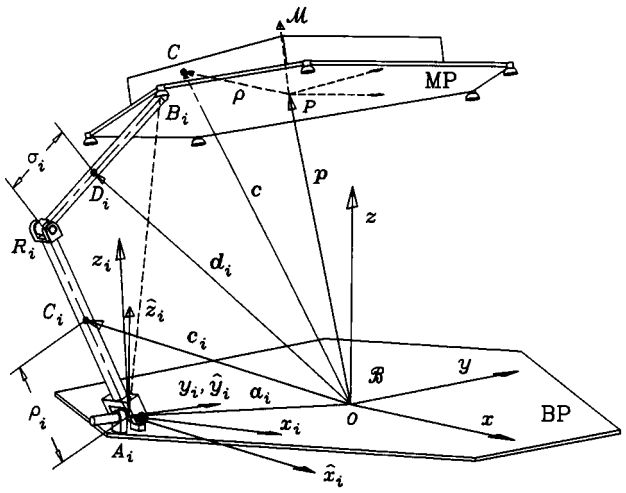

Fig. 5. Kinematic notation for the dynamic analysis.

At this stage, we assign body frames $\mathcal{G}_i$ and $\mathcal{H}_i$ to the two links of the ith leg, for $i = 1, \ldots, 6$. The origins of these frames are fixed at points A_i and R_i, respectively, such that the rotation matrices, $\boldsymbol{G}_i$ and $\boldsymbol{H}_i$, representing the orientations of $\mathcal{G}_i$ and $\mathcal{H}_i$ with respect to $\mathcal{B}$, are defined as

$$\boldsymbol{G}_i \equiv [\boldsymbol{x}_i, \boldsymbol{e}_i \times \boldsymbol{x}_i, \boldsymbol{e}_i]; \quad \boldsymbol{H}_i \equiv [\boldsymbol{x}_i, \boldsymbol{s}_i \times \boldsymbol{x}_i, \boldsymbol{s}_i] \tag{40}$$

where $\boldsymbol{e}_i \equiv \hat{\boldsymbol{Q}}_i \boldsymbol{Q}_i [\boldsymbol{e}_i]_i$ and $\boldsymbol{s}_i \equiv \hat{\boldsymbol{Q}}_i \boldsymbol{Q}_i [\boldsymbol{s}_i]_i$. Now, upon differentiating equations (39a–c) with respect to time, for $i = 1, \ldots, 6$, we obtain

$$\dot{\boldsymbol{c}}_i = \rho_i \dot{\hat{\boldsymbol{Q}}}_i \{\boldsymbol{\Omega}_i \boldsymbol{Q}_i [\boldsymbol{e}_i]_i + \boldsymbol{Q}_i [\dot{\boldsymbol{e}}_i]_i\} \tag{41a}$$

$$\dot{\boldsymbol{d}}_i = \dot{\hat{\boldsymbol{Q}}}_i \boldsymbol{\Omega}_i \boldsymbol{Q}_i \{l_i [\boldsymbol{e}_i]_i + \sigma_i [\boldsymbol{s}_i]_i\} + \hat{\boldsymbol{Q}}_i \boldsymbol{Q}_i \{l_i [\dot{\boldsymbol{e}}_i]_i + \sigma_i [\dot{\boldsymbol{s}}_i]_i\} \tag{41b}$$

$$\dot{\boldsymbol{c}} = \dot{\boldsymbol{p}} + \boldsymbol{\Omega} \boldsymbol{Q} \boldsymbol{\rho} \tag{41c}$$

in which

$$[\dot{\boldsymbol{e}}_i]_i \equiv \frac{d}{dt} [\boldsymbol{e}_i]_i = [0, -\sin \psi_i, \cos \psi_i]^T \dot{\psi}_i \tag{42a}$$

$$[\dot{\boldsymbol{s}}_i]_i \equiv \frac{d}{dt} [\boldsymbol{s}_i]_i = [0, \sin (\psi_i + \theta_i), -\cos (\psi_i + \theta_i)]^T (\dot{\psi}_i + \dot{\theta}_i) \tag{42b}$$

Further differentiation of equations (41a–c) with respect to time leads to the relations below:

$$\ddot{\boldsymbol{c}}_i = \rho_i \dot{\hat{\boldsymbol{Q}}}_i \{(\dot{\boldsymbol{\Omega}}_i + \boldsymbol{\Omega}_i^2) \boldsymbol{Q}_i [\boldsymbol{e}_i]_i + 2\boldsymbol{\Omega}_i \boldsymbol{Q}_i [\dot{\boldsymbol{e}}_i]_i + \boldsymbol{Q}_i [\ddot{\boldsymbol{e}}_i]_i\} \tag{43a}$$

$$\ddot{\boldsymbol{d}}_i = \ddot{\hat{\boldsymbol{Q}}}_i \{(\dot{\boldsymbol{\Omega}}_i + \dot{\boldsymbol{\Omega}}^2) \boldsymbol{Q}_i (l_i [\boldsymbol{e}_i]_i + \sigma_i + [\boldsymbol{s}_i]_i) + 2\boldsymbol{\Omega}_i \boldsymbol{Q}_i (l_i [\dot{\boldsymbol{e}}_i]_i + \sigma_i [\dot{\boldsymbol{s}}_i]_i) + \boldsymbol{Q}_i (l_i [\ddot{\boldsymbol{e}}_i]_i + \sigma_i [\ddot{\boldsymbol{s}}_i]_i)\} \tag{43b}$$

$$\ddot{\boldsymbol{c}} = \ddot{\boldsymbol{p}} + (\dot{\boldsymbol{\Omega}} + \boldsymbol{\Omega}^2) \boldsymbol{Q} \boldsymbol{\rho} \tag{43c}$$

In the above relations, $[\ddot{\boldsymbol{e}}_i]_i$ and $[\ddot{\boldsymbol{s}}_i]_i$ are readily computed from equations (42a–b) by direct differentiation with respect to time. Similarly, from equation (12) we have

$$\dot{\boldsymbol{\omega}}_i \equiv [0, -\ddot{\varphi}_i, 0]^T = \text{vect} (\dot{\boldsymbol{\Omega}}_i) \tag{44}$$

On the other hand, the generalized gravity wrench $\boldsymbol{w}^g$ can be expressed in the form

$$\boldsymbol{w}^g = [(\boldsymbol{w}_1^g)^T, \ldots, (\boldsymbol{w}_6^g)^T, (\boldsymbol{w}_{6+1}^g)^T, \ldots, (\boldsymbol{w}_{6+6}^g)^T, (\boldsymbol{w}_M^g)^T]^T \tag{45}$$

where, $(\boldsymbol{w}_i^g) \equiv [\boldsymbol{0}^T, m_i \boldsymbol{g}^T]$, $(\boldsymbol{w}_{6+i}^g)^T \equiv [\boldsymbol{0}^T, m_{6+i} \boldsymbol{g}^T]$, with m_i and m_{6+i} representing the mass of the first and second link of the ith leg, respectively. Moreover, $\boldsymbol{w}_M^g \equiv [\boldsymbol{0}^T, m\boldsymbol{g}^T]$, $\boldsymbol{g} \equiv [0, 0, -g]^T$, with m representing the mass of the MP and g denoting the gravity constant. Now, let the inertia matrices of the leg links and the MP in their associated body frames $\mathcal{G}_i$, $\mathcal{H}_i$ and $\mathcal{M}$, be denoted by $[\boldsymbol{I}_i]_{\mathcal{G}}$, $[\boldsymbol{I}_{6+i}]_{\mathcal{H}}$, for $i = 1, \ldots, 6$, and $[\boldsymbol{I}_M]_{\mathcal{M}}$, respectively. Then, they can be transformed into frame $\mathcal{B}$ using the relations below:

$$\boldsymbol{I}_i = \boldsymbol{G}_i [\boldsymbol{I}_i]_{\mathcal{G}} \boldsymbol{G}_i^T; \quad i = 1, \ldots, 6 \tag{46a}$$

$$\boldsymbol{I}_{6+i} = \boldsymbol{H}_i [\boldsymbol{I}_{6+i}]_{\mathcal{H}} \boldsymbol{H}_i^T; \quad i = 1, \ldots, 6 \tag{46b}$$

$$\boldsymbol{I}_M = \boldsymbol{Q} [\boldsymbol{I}_M]_{\mathcal{M}} \boldsymbol{Q}^T; \tag{46c}$$

It should be noted that the twist t_C of the mass center of the MP can be related to the actuated joint-rate vector, $\dot{\boldsymbol{\varphi}}$, simply by replacing $\boldsymbol{Q}\boldsymbol{b}_i$ in equation (21) by $\boldsymbol{Q}\boldsymbol{b}_i - \boldsymbol{\rho}$, for $i = 1, \ldots, 6$. In this way, the inverse Jacobian of the manipulator remains unchanged, while the direct Jacobian with respect to point C, i.e., $\boldsymbol{B}_C$, changes to

$$\boldsymbol{B}_C = \begin{bmatrix} [\boldsymbol{Q}(\boldsymbol{b}_1 - \boldsymbol{\rho}) \times \boldsymbol{x}_1]^T & \boldsymbol{x}_1^T \\ \vdots & \vdots \\ [\boldsymbol{Q}(\boldsymbol{b}_6 - \boldsymbol{\rho}) \times \boldsymbol{x}_6]^T & \boldsymbol{x}_6^T \end{bmatrix} \tag{47}$$

3.2 Numerical evaluation of the NOC

The direct derivation of $\boldsymbol{T}$ from equation (32a) is, in general, very tedious and increases the complexity of the dynamics problem. Thus, we resort to the method proposed by Ma[9] to calculate $\boldsymbol{T}$ numerically, which we briefly recall, as applied to the manipulator under study.

At the outset, we let $\boldsymbol{\delta}_j$ denote the jth column of $\boldsymbol{T}$ and notice that $\boldsymbol{T}$ is independent of the vector of actuated joint rates, $\dot{\boldsymbol{\varphi}}$. On the other hand, the generalized twist vector can be expressed as a linear combination of $\boldsymbol{\delta}_j$, for $j = 1, \ldots, 6$. Hence, one can infer that $\boldsymbol{\delta}_j$ is equal to $\boldsymbol{t}$ when $\dot{\varphi}_j$ is equal to unity and all other components of $\dot{\boldsymbol{\varphi}}$ are zero, i.e.

$$\boldsymbol{\delta}_j = \boldsymbol{t}(\boldsymbol{\varphi}, \dot{\boldsymbol{\varphi}}), \; |_{\dot{\varphi}_1 = 0, \ldots, \dot{\varphi}_{j-1} = 0, \dot{\varphi}_j = 1, \dot{\varphi}_{j+1} = 0, \ldots, \dot{\varphi}_6 = 0} \tag{48}$$

which means that matrix $\boldsymbol{T}$ can be numerically calculated columnwise for all leg links. In the case of the MP, the corresponding $\boldsymbol{T}$ can be directly computed using equations (23 & 47), i.e. as $\boldsymbol{B}_C^{-1} \boldsymbol{A}$.

4 IMPLEMENTATION AND A NUMERICAL EXAMPLE

The preceding kinematics and dynamics modeling can be incorporated into a single algorithm to evaluate the kinematics and dynamics of the manipulator under different end-effector Cartesian trajectories or actuator force histories. For simulation purposes, the basic steps of this algorithm for the inverse problem are described in

https://doi.org/10.1017/S0263574797000477 Published online by Cambridge University Press

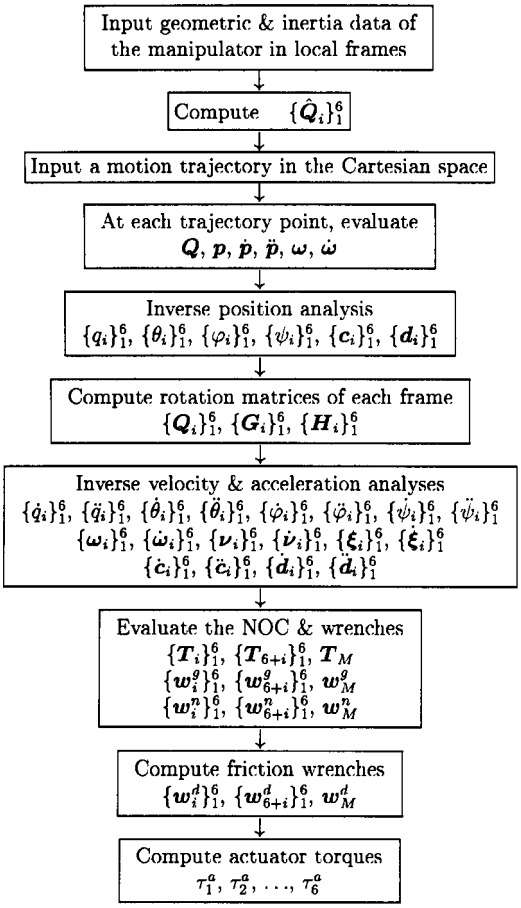

Fig. 6. Algorithm for the inverse dynamics of the manipulator.

the diagram shown in Figure 6. The formulas corresponding to each block of the diagram have been introduced in the previous sections and, hence, will not be discussed further.

4.1 Numerical example

A numerical example of the inverse dynamics is included in this section. The geometric information of the manipulator used in this example is given in Table 1. The length of the leg links, the location of the mass centers, the mass of each body and their associated inertia properties, for $i = 1, \ldots, 6$, are as follows:

$$\{l_i\}_1^6 = \{s_i\}_1^6 = 1.4 \text{ (m)}$$

$$\{\rho_i\}_1^6 = \{\sigma_i\}_1^6 = 0.7 \text{ (m)}$$

$$\boldsymbol{\rho} = [0, 0, 1.88]^T \quad \text{(m)}$$

$$[\boldsymbol{I}]_{\mathcal{G}} = \begin{bmatrix} 4.2 & 0 & 0 \\ 0 & 4.2 & 0 \\ 0 & 0 & 0.015 \end{bmatrix} \text{ (kg-m}^2\text{)}, \quad m_i = 10 \text{ (kg)};$$

$$[\boldsymbol{I}_{6+i}]_{\mathcal{H}} = \begin{bmatrix} 3.3 & 0 & 0 \\ 0 & 3.3 & 0 \\ 0 & 0 & 0.015 \end{bmatrix} \text{ (kg-m}^2\text{)}, \quad m_{6+i} = 10 \text{ (kg)};$$

$$[\boldsymbol{I}_M]_{\mathcal{M}} = \begin{bmatrix} 800 & 0 & 0 \\ 0 & 800 & 0 \\ 0 & 0 & 800 \end{bmatrix} \text{ (kg-m}^2\text{)}, \quad m = 500 \text{ (kg)}$$

We have generated a helical trajectory in the Cartesian space, as described in the Appendix. The motion of the manipulator is such that point P remains on this trajectory while the MP maintains a fixed orientation with respect to the Frenet-Serret triad of the helix (see Figs. 7 and 8). The corresponding time-histories of the

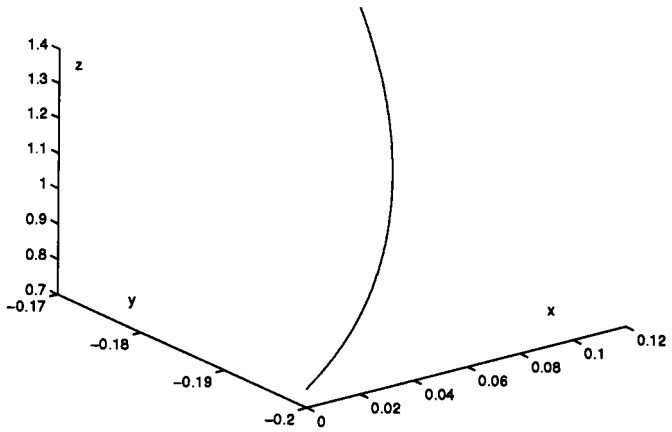

Fig. 7. Trajectory of point P.

Table I. The parameters of the BP and MP (meter).

i	1	2	3	4	5	6
$\boldsymbol{u}_i$	−0.9397	0.9397	0.4698	−0.4698	0.4698	−0.4698
	0	0	−0.8138	0.8138	0.8138	−0.8138
	0.3420	0.3420	0.3420	0.3420	0.3420	0.3420
$\boldsymbol{a}_i$	−0.0953	0.0953	1.7521	1.6568	−1.6568	−1.7521
	−1.9682	−1.9682	0.9016	1.0666	1.0666	0.9016
	0	0	0	0	0	0
$\boldsymbol{b}_i$	−0.0667	0.0667	1.2265	1.1598	−1.1598	−1.2265
	−1.3847	−1.3777	0.6381	0.7536	0.7466	0.6311
	0	0	0	0	0	0

https://doi.org/10.1017/S0263574797000477 Published online by Cambridge University Press

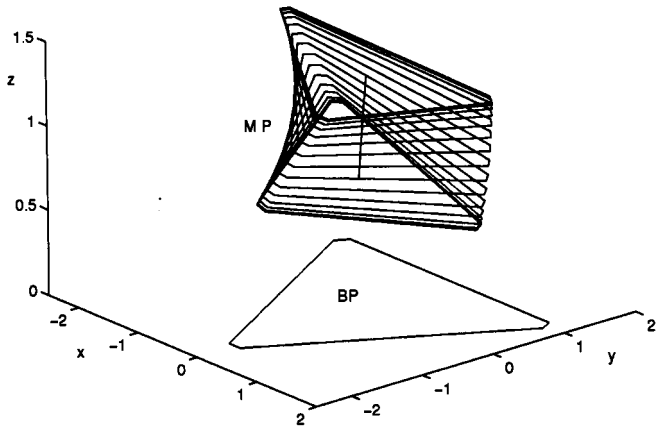

Fig. 8. Poses of the MP while tracing the helical trajectory.

components of the acceleration vector of point P and angular acceleration vector of the MP are shown in Figures 9 and 10, respectively. Moreover, the time-histories of the unactuated joint variables, i.e., $\{\psi_i\}_1^6$ and $\{\theta_i\}_1^6$, and also the actuated joint variables $\{\varphi_i\}_1^6$ can be seen in Figures 11, 12, and 13, respectively. As well, the corresponding actuator torques $\{\tau_i^a\}_1^6$ are given in Figure 14. These results have been obtained by

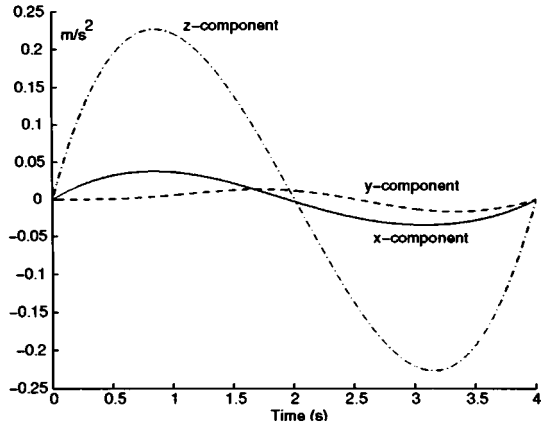

Fig. 9. Time-histories of the components of the acceleration vector of point P.

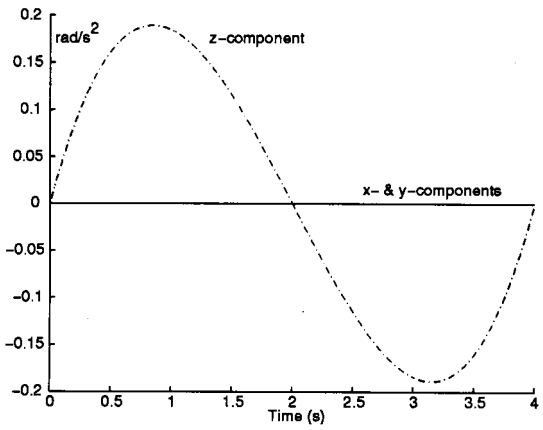

Fig. 10. Time-histories of the components of the angular acceleration vector of the MP.

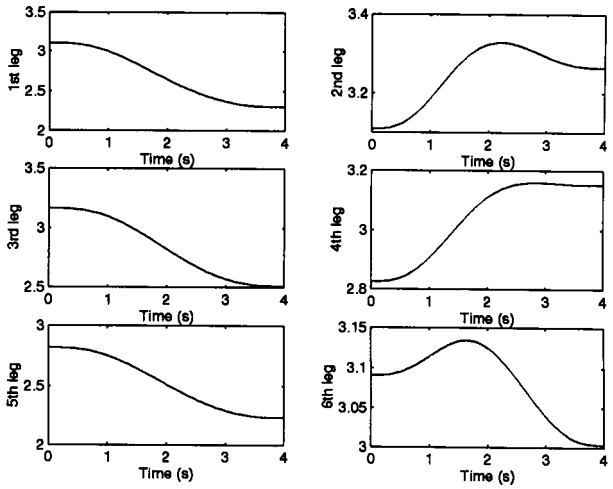

Fig. 11. Time-histories of the unactuated joint variables $\{\psi_i\}_1^6$ (rad).

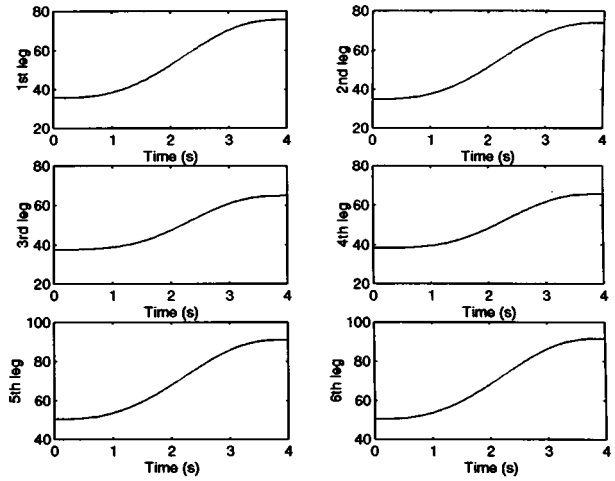

Fig. 12. Time-histories of the unactuated joint variables $\{\theta_i\}_1^6$ (deg).

assuming that the dissipative effects can be neglected, as compared with the other forces involved.

5 CONCLUSIONS

In this paper, the kinematics and dynamics of a six-dof parallel manipulator with six revolute legs were studied.

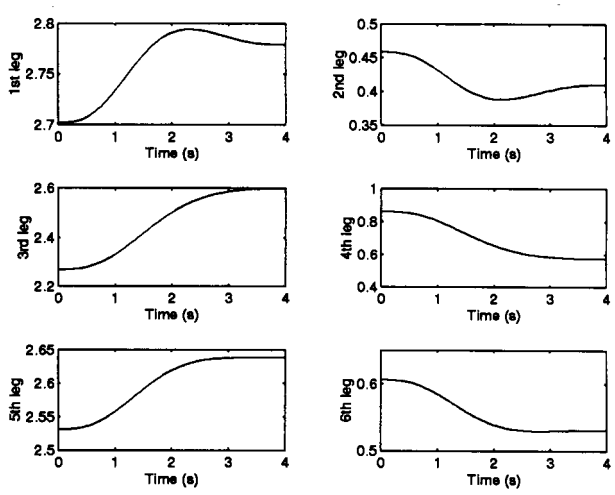

Fig. 13. Time-histories of the actuated joint variables $\{\varphi_i\}_1^6$ (rad).

https://doi.org/10.1017/S0263574797000477 Published online by Cambridge University Press

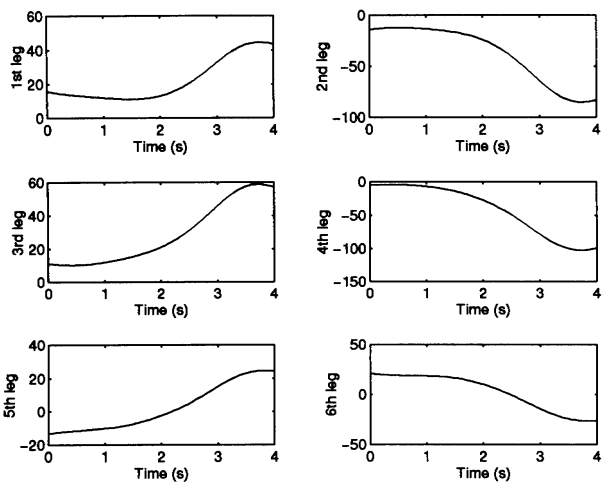

Fig. 14. Time-histories of the joint torques $\{\tau_i^a\}_1^6$ (kNm).

Each leg comprises two links connected by a revolute joint and is actuated by a motor at the base. In this way, the leg masses and inertias can be reduced significantly. To study the motion characteristics of the manipulator, we introduced a kinematic model that was used to derive the dynamics equations of the system based on the method of the NOC. The present study provides a framework for future research on the design and control of this type of manipulators. Moreover, the study can further reveal the potential applications of the proposed mechanism as a robotic manipulator, a motion simulator, and so on.

Acknowledgments

The work reported here was possible under research grants from Canada's *Natural Sciences and Engineering Research Council* (NSERC) and Quebec's *Fonds pour la formation de chercheurs et l'aide à la recherche* (FCAR). The first author acknowledges the support of NSERC through a Postdoctoral Research Fellowship. The second author acknowledges the support of Italy's *Consiglio Nazionale delle Ricerche* (CNR).

References

1. D. Stewart, "A Platform with Six Degrees of Freedom" *Proc. Inst. Mech. Engr.* **180,** Part 1, No. 15, 371–378 (1965).
2. K. Cleary and T. Brooks, "Kinematic Analysis of a Novel 6-DOF Parallel Manipulator" *Proc. 1993 IEEE International Conference on Robotics and Automation,* Atlanta (1993) pp. 708–713.
3. J-P. Merlet, *Les Robots Parallèles* (Habilitation Diriger des Recherches, University of Nice, 1993).
4. K. Sugimoto, "Kinematic and Dynamic Analysis of Parallel Manipulators by Means of Motor Algebra" *ASME J. Mechanisms, Transmissions, and Automation in Design* **109,** 3–7 (1987).
5. W.Q.D. Do and D.C.H. Yang, "Inverse Dynamic of a Platform Type of Robot" *J. Robotic Systems* **5,** No. 3, 210–227 (1988).
6. J.C. Hudgens and D. Tesar, "A Fully-Parallel Six Degree-of-Freedom Micromanipulator: Kinematic Analysis and Dynamic Model" *Proc. ASME Design Tech. Conf.,* Kissimme (1988) pp. 29–37.
7. K.M. Lee and D.K. Shah, "Dynamic Analysis of a Three-Degrees-of-Freedom In-Parallel Actuated Manipulator" *IEEE Trans. Robotics and Automation* **4,** No. 3, 361–367 (1988).
8. K. Sugimoto, "Computational Scheme for Dynamic Analysis of Parallel Manipulators" *ASME J. Mechanisms, Transmissions, and Automation in Design* **111,** 29–33 (1989).
9. O. Ma, "Mechanical Analysis of Parallel Manipulators with Simulation, Design and Control Applications" *Ph.D. Thesis* (McGill University, Montreal, 1991).
10. Z. Huang and H.B. Wang, "Dynamic Force Analysis of *n*-d.f. Multiloop Complex Spatial Mechanisms" *Mech. Mach. Theory* **27,** No. 1, 97–105 (1992).
11. F. Pierrot, A. Fournier and P. Dauchez, "Toward a Fully Parallel 6-DOF Robot for High-Speed Applications" *Int. J. Robotics and Automation* **7,** No. 1, 15–22 (1992).
12. C.D. Zhang and S.M. Song, "An Efficient Method for Inverse Dynamics of Manipulators Based on the Virtual Work Principle" *J. Robotics Systems* **10,** No. 5, 605–627 (1993).
13. G.H. Pfreundschuh, T.G. Sugar and V. Kumar, "Design and Control of a Three-Degrees-of-Freedom in-Parallel, Actuated Manipulator" *J. Robotic Systems* **11,** No. 2, 103–115 (1994).
14. K.W. Lilly and D.E. Orin, "Efficient Dynamic Simulation of Multiple Chain Robotic Mechanisms" *ASME J. Dynamic Systems, Measurement, and Control* **116,** 223–231 (1994).
15. J. Angeles and S. Lee, "The Formulation of Dynamical Equation of Holonomic Mechanical Systems Using a Natural Orthogonal Complement" *ASME J. Applied Mechanics* **55,** 243–244 (1988).
16. J. Angeles and S. Lee, "The Modeling of Holonomic Mechanical Systems Using a Natural Orthogonal Complement" *Trans. Canadian Society of Mechanical Engineers* **13,** No. 4, 81–89 (1989).
17. C. Gosselin and J. Angeles, "Singularity Analysis of Closed-Loop Kinematic Chains" *IEEE Trans. Robotics and Automation* **6,** No. 3, 281–290 (1990).
18. T.R. Kane and D.A. Levinson, *Dynamics*: *Theory and Applications* (McGraw-Hill, New York, 1985).
19. D.J. Struik, *Lectures on Classical Differential Geometry* (Addison-Wesley Publishing Co., Reading., Mass., 1961).

APPENDIX

To generate a sample trajectory in the Cartesian space, we let the position vector of point P of the MP be defined in frame $\mathcal{B}$ by a vector-valued function that represents the position vector of a point of a helix, namely,

$$\boldsymbol{p} = a\cos(\beta+\omega)\boldsymbol{e}_x + a\sin(\beta+\omega)\boldsymbol{e}_y + b(\beta+\bar{\omega})\boldsymbol{e}_z; \quad a>0,\ b\neq 0 \tag{49}$$

where a, b, ω, and $\bar{\omega}$ are scalar constants; the first two with units of length, the last two dimensionless. Moreover, $\boldsymbol{e}_x$, $\boldsymbol{e}_y$ and $\boldsymbol{e}_z$ are unit vectors along the three axes of frame $\mathcal{B}$, while β denotes the parameter of the helix that varies with time t according to the quintic polynomial below:

$$\beta = \sum_{k=0}^{5} a_k t^k \tag{50}$$

Moreover, if the motion of the manipulator starts at time

https://doi.org/10.1017/S0263574797000477 Published online by Cambridge University Press

$t = 0$ and ends at time $t = t_f$, then the coefficients $\{a_k\}_0^5$ are given as

$$a_0 = \beta_0; \quad a_1 = \dot{\beta}_0; \quad a_2 = \frac{1}{2}\ddot{\beta}_0 \tag{51a}$$

$$a_3 = \frac{20\beta_f - 20\beta_0 - (8\dot{\beta}_f + 12\dot{\beta}_0)t_f - (3\ddot{\beta}_0 - \ddot{\beta}_f)t_f^2}{2t_f^3} \tag{51b}$$

$$a_4 = \frac{30\beta_0 - 30\beta_f + (14\dot{\beta}_f + 16\dot{\beta}_0)t_f + (3\ddot{\beta}_0 - 2\ddot{\beta}_f)t_f^2}{2t_f^4} \tag{51c}$$

$$a_5 = \frac{12\beta_f - 12\beta_0 - (6\dot{\beta}_f + 6\dot{\beta}_0)t_f - (\ddot{\beta}_0 - \ddot{\beta}_f)t_f^2}{2t_f^5} \tag{51d}$$

where subscripts "0" and "f" represent values of the corresponding parameters at times $t = 0$ and $t = t_f$, respectively. Furthermore, to start and end the motion with zero velocity and acceleration, we set $\dot{\beta}_0 = \ddot{\beta}_0 = \dot{\beta}_f = \ddot{\beta}_f = 0$. Now, upon differentiating equation (49) twice with respect to time, we obtain

$$\dot{\boldsymbol{p}} = \boldsymbol{m}\dot{\beta}; \quad \ddot{\boldsymbol{p}} = \boldsymbol{m}\ddot{\beta} + \boldsymbol{n}\dot{\beta}^2 \tag{52}$$

where $\boldsymbol{m}$ and $\boldsymbol{n}$ are defined as

$$\boldsymbol{m} \equiv -a\sin(\beta + \omega)\boldsymbol{e}_x + a\cos(\beta + \omega)\boldsymbol{e}_y + b\boldsymbol{e}_z$$
$$\boldsymbol{n} \equiv -a\cos(\beta + \omega)\boldsymbol{e}_x - a\sin(\beta + \omega)\boldsymbol{e}_y$$

and $\dot{\beta}$ and $\ddot{\beta}$ are computed upon differentiating equation (50) twice with respect to time, as

$$\dot{\beta} = \sum_{k=0}^{5} k a_k t^{k-1}; \quad \ddot{\beta} = \sum_{k=0}^{5} k(k-1) a_k t^{k-2} \tag{53}$$

On the other hand, expressions for the angular velocity and angular acceleration vectors of the MP can be derived using the *Darboux* vector and its time-derivative associated with the helical parametric curve,[19] i.e. $\boldsymbol{\omega} = \dot{\beta}\boldsymbol{e}_z$ and $\dot{\boldsymbol{\omega}} = \ddot{\beta}\boldsymbol{e}_z$. Moreover, the unit tangent, normal, and binormal vectors defining the Frenet-Serret triad of the helix are derived as

$$\boldsymbol{e}_t = \frac{1}{(a^2 + b^2)^{1/2}}\boldsymbol{m}; \quad \boldsymbol{e}_n = \frac{1}{a}\boldsymbol{n}; \quad \boldsymbol{e}_b = \boldsymbol{e}_t \times \boldsymbol{e}_n \tag{54}$$

Hence, the rotation matrix $\boldsymbol{Q}$ is expressed in the form

$$\boldsymbol{Q} = [-\boldsymbol{e}_b, \boldsymbol{e}_n, \boldsymbol{e}_t] \tag{55}$$

For the purpose of the present study, we assigned the following values to the parameters involved:

$$\beta_0 = -\pi/2, \quad \beta_f = -\pi/3, \quad a = 0.2,$$
$$b = 1.2, \quad \omega = 0, \quad \bar{\omega} = 2.2$$

https://doi.org/10.1017/S0263574797000477 Published online by Cambridge University Press